JOTCS A
Journal of the Turkish Chemical Society
Section: A
Chemistry
TURKISH CHEMICAL SOCIETY

Preparation of α-Al_2O_3 Supports for Thin Membrane Fabrication

Berna Topuz*, Ali Semih Yurttaş, Ali Altunsoy

Ankara University, Chemical Engineering Department, 06100, Ankara, Turkey

Abstract: In this study, macroporous α-alumina supports were prepared by using vacuum assisted filtration of α-Al_2O_3 suspensions with different particle size. The average particle sizes of the powders are 400 and 200 nm. The prepared supports had smooth and uniform surface microstructure and well suited for the fabrication of thin continuous membrane. The microstructure consists of a random close-packing of 200 nm particles led to improved surface uniformity and roughness. ZnO spheres were prepared by homogeneous precipitation and added to the colloidal suspension to modify the support structure and increase the support flux. Structural parameters such as pore diameter and tortuosity of the prepared macroporous supports were estimated by using He, N_2, CO_2 permeance measurements. Slight pressure dependence in the permeance values indicated the contribution of viscous flow to the Knudsen flow. The supports prepared by alumina powder with a larger particle size exhibited a He permeance of three times higher than that of prepared with a smaller particle size. The addition of ZnO resulted in the increase in He permeance value significantly for the support prepared by 400 nm particles in size. He permeance was in a range of 8.5-8.7x10^{-6} mol/(m^2sPa) which is very close to the desired value of 1x10^{-5} mol/(m^2sPa).

Keywords: Membrane, support, alumina, high flux, colloidal processing, ZnO.

Submitted: November 14, 2017. **Accepted:** . December 19, 2017.

Cite this: Topuz B, Yurttaş A, Altunsoy A. Preparation of alpha-Al2O3 Supports for Thin Membrane Fabrication. JOTCSA. 2018;5(1):191–204.

DOI: http://dx.doi.org/10.18596/jotcsa.351708.

***Corresponding author. E-mail:** topuzb@ankara.edu.tr.

INTRODUCTION

Due to the high energy demand in our developing world, designing more energy-efficient processes is one of the significant challenges over the past few decades. Separation-based technologies play a significant role in chemical industries and account for 15% of world's energy consumption (1). Membrane-based separations are attractive in various separation processes due to their low energy consumption and operating cost over other thermally driven separation techniques like distillation. The intense interest towards thermally and mechanically stable ultrathin supported membranes (like zeolite, sol-gel derived ceramic, and MOF) with molecular sieving capability is continuously increasing due to their potential to attain high throughput. The mostly used supported membrane structure is composed of layers with a gradual decrease in pore size and thickness on a macroporous support to minimize the gas resistance through the membrane (2).

The macroporous supports are designed to mechanically hold the thin separative membrane layer and must be chemically inert, thermally stable, and highly permeable. The fabrication of ultrathin supported membranes necessitate the desired surface characteristics of support in terms of roughness and homogeneity. Ultrathin membranes (<500 nm in thickness) on macroporous supports have been prepared for high flux gas separation, vapor permeation, and pervaporation applications (3-6).

Ceramic supports have advantages in terms of their thermal stability and gas flux compared to their polymeric counterparts (7-9). One important disadvantage of macro/mesoporous ceramic supports is their high cost that impedes large scale deployment of thermally stable ceramic/zeolite/MOF membranes. Silica, zirconia, titania, and alumina or their composites are generally used as the membrane support materials (9-13). The supports must be highly porous so the molecules that were released through the membrane layer can also easily pass through the supports without any resistant. They must also be mechanically strong and have a smooth surface for the formation of defect-free continuous thin membrane layer.

Dry pressing, tape casting, and extrusion are the generally used methods for the preparation of ceramic membrane supports, however colloidal processing (slip casting/vacuum-assisted filtration) of statically or sterically stable suspensions allow the fabrication of macroporous supports with appropriate surface properties (14, 15). A smoother surface with less amount of roughness can be obtained by vacuum filtration method in which colloidal processing is used (15). High throughput thin membranes necessitate high flux membrane support with homogeneous surface properties, uniform

pore size and macro-defect free surface. The support structure has a great importance for determining the membrane microstructure, membrane performance in terms of selectivity and flux.

In this study, disk-shaped alumina supports with 21 mm in diameter and ~2 mm in thickness were prepared through colloidal processing of α-Al_2O_3 powders with different particle size (Baikowski CR-6 and Sumitomo Chemical AKP-50). ZnO spheres were added to the structure in order to increase the permeability of the supports. Single gas (He, N_2, CO_2) permeation behavior of the supports was determined at different temperature and pressure. Structural parameters of prepared supports were also estimated by single gas permeance measurements.

MATERIALS AND METHODS

Preparation of ZnO

ZnO nanospheres were prepared by homogeneous precipitation at 160 °C for 2 hours (16). Zinc acetate dihydrate (Sigma-Aldrich) was dissolved in diethylene glycol (DEG, Merck) with molar ratio of 1:105.4 DEG. After cooling the synthesis solution to the room temperature, ZnO spheres were collected by centrifugation (10000 rpm for 15 min). The ZnO spheres were washed 3 times with ethanol and dispersed in ethanol to be further used in α-Al_2O_3 support preparation.

Support Preparation

CR-6 (Baikowski) and AKP-50 (Sumitomo Chemical Company) α-Al_2O_3 powders were used to prepare macroporous supports with a thickness and diameter of 2 mm and 21 mm, respectively. The properties of these powders are shown in Table 1.

Electrostatically stable suspensions were first prepared by dispersing the powders in deionized water at pH~2. Electrostatic stability can be provided in aqueous suspension at pH in the 2–3 range for positively charged alumina particles (14). Nitric acid solution (1.44 M) was used for the adjustment of pH. Stable suspensions with 20 vol% Al_2O_3 in water were horn-sonicated (Sonics Vibra-Cell VCX130, 130 watts, 0.250'' probe) with an operating power at 80% maximum amplitude, 2 seconds of pause for each 5 seconds sonication sequences for 3 minutes. The suspensions were filtered with 1 μm stainless steel mesh and 3 μL/g-powder n-octanol was added prior to bath sonication at degassing mode for 90 minutes to eliminate the air bubbles in the suspension. ZnO added alumina supports were prepared by adding ZnO spheres into alumina suspension before casting. The amount of ZnO was kept at 3 wt% with respect to the weight of alumina. The presence of ZnO was

expected to modify the pore structure and increase the support flux. The supports were encoded according to their powder particle size and whether they had ZnO (Table 1).

Table 1: Support codes and properties of α-Al_2O_3 powders.

Support Code	Powder Type	Mean Particle Size (nm)	BET Surface Area (m^2/g)	ZnO Addition
S400	Baikowski /CR-6	400	6	-
S200	Sumitomo Chemical/AKP-50	200	10.3	-
S400-Z	Baikowski /CR-6			3 wt%
S200-Z	Sumitomo Chemical/AKP-50			3 wt%

Polypropylene cylinder molds (22 mm inner dimension, 70 mm height) were used for casting the supports. The molds were placed vertically on a 0.22 μm nylon membrane (Advantec MFS, Inc.) under partial vacuum (-0.6 bar). Alumina and ZnO-added alumina green compacts were removed from the molds after 2 hours of vacuum filtration and dried overnight at room temperature. The surfaces of the supports were cleaned with pressurized nitrogen (1 bar) before heat treatment. Dried compacts of S400, S400-Z and S200, S200-Z were heat treated at 1000 °C and 900 °C for 3 hours with a heating and cooling rate of 5 °C/min, respectively. The preparation of ZnO-added alumina supports is given schematically in Figure 1.

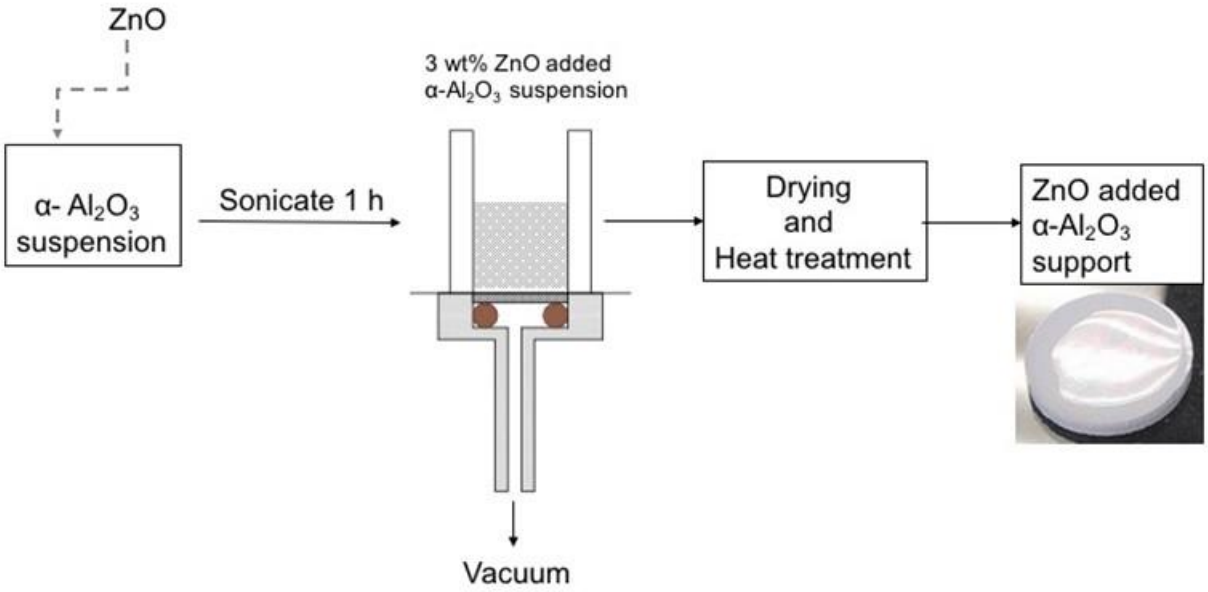

Figure 1: A schematic representation for the preparation of ZnO-added alumina supports.

Characterization

The morphology and size of the ZnO crystals were determined by field emission Scanning Electron Microscopy (SEM, QUANTA 400F). The samples were sputter coated with a thin

layer of Au-Pd before analysis. After degassing at 250 °C for 4 hours, BET surface area of the ZnO spheres were obtained from N_2 adsorption-desorption isotherms (AUTOSORB-6B).

The microstructure of the top and cross-section of the prepared supports were investigated by Scanning Electron Microscopy (SEM - Zeiss EVO 40 and QUANTA 200 FEG). The elemental composition was determined by Energy Dispersive X-ray Spectroscopy. Pore size and pore volume of the supports were determined with Mercury Intrusion Porosimeter (Quantachrome Corporation, Poremaster 60).

Gas Permeation

Single gas permeation of He, N_2 and CO_2 through the prepared supports were determined by using a constant pressure-variable volume membrane test system. The pressure of the feed side was adjusted in order to obtain transmembrane pressures in the 1-3 bar range and kept constant during the permeation experiments. Permeate flow rates were measured for the determination of single gas permeance (mol/m^2-s-Pa) values at different temperatures (25 °C-150 °C) for a constant transmembrane pressure of 1 bar.

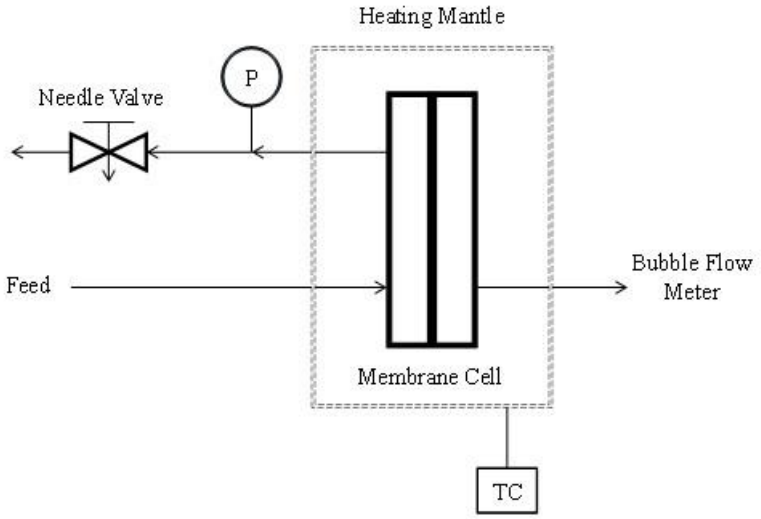

Figure 2: Single gas membrane test system.

RESULTS AND DISCUSSION

ZnO spheres with a bimodal particle size distribution were synthesized by precipitation. Figure 3.a shows a SEM image of ZnO spheres. The average sphere sizes were estimated from the SEM image as 680±64 nm and 290±90 nm for large and small spheres, respectively. SEM image with high magnification (Figure 3.a, inset) clearly shows that these spheres have rough surfaces. The nitrogen sorption–desorption isotherms of the spheres at 77 K showed a Type IV isotherm with a H2 hysteresis loop (Figure 3.b) indicating the mesoporous nature of ZnO spheres. BET surface area and pore volume of the sample

were 52 m^2/g and 0.075 cm^3/g, respectively.

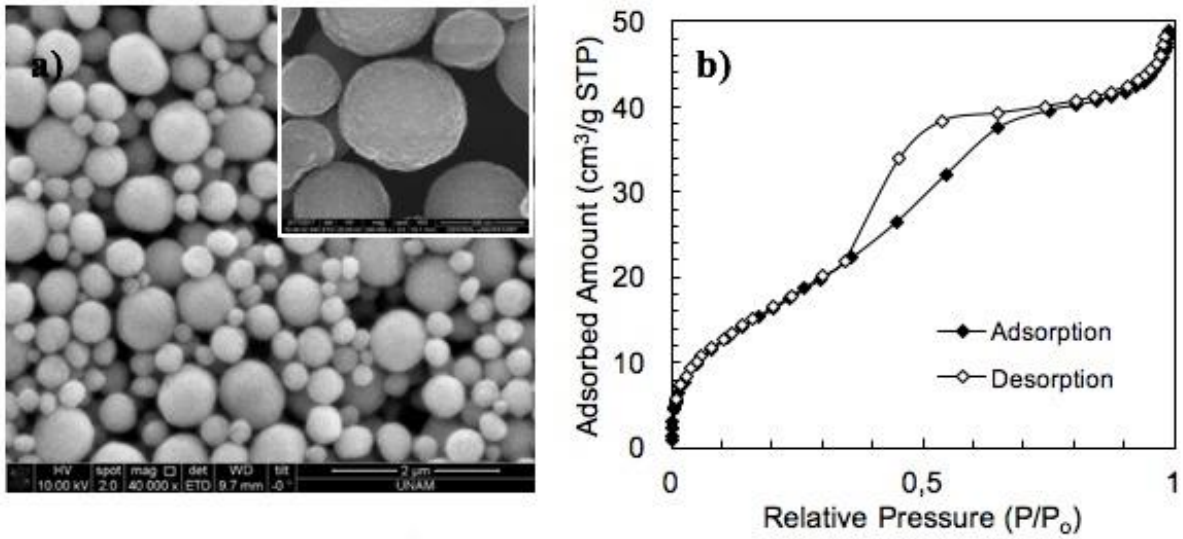

Figure 3: (a) SEM micrographs (inset: 200 kX) and (b) N_2 adsorption-desorption isotherms of ZnO spheres.

The microstructure of the support before heat treatment can be controlled by the colloidal stability of the suspension. Different colloidal approaches can be used to stabilize the particles in suspensions; *electrostatic stabilization, steric stabilization* and *electrosteric stabilization* (17). To fabricate the support with homogeneous improved properties, colloidal processing of electrostatically stabilized alumina suspension was used. Smooth and homogeneous support surface with roughness less than the membrane thickness is desirable for defect free, continuous thin film formation. Figure 4 shows SEM images of supports prepared by vacuum filtration. We did not observe any surface defects like a print of gas bubbles in the suspension, contamination with a foreign particles or abnormal grain growth. Low surface roughness with well packed particles have been obtained for both supports. Open pore structures were obtained for both types of supports without any partial closure of the surface pores. Figure 4.b shows SEM image of top surface of S200 support which is prepared by suspension with a smaller average particle size. The surface of this support is much smoother and densely packed than that prepared by a larger average particle size (Figure 4.b). Smooth and uniform surface properties may be attributed to the colloidal stability of particles in the suspension. However, the extent of such a large particle stability could be enhanced by using different colloidal approach. A graded morphology through the fracture cross-section of the supports can be seen in Figure 4.c and Figure 4.d. This structure is highly desirable to fabricate high flux crack-free thin membranes with high selectivity. Particle size distribution in the suspensions has a strong impact on the formation of this structure since the smaller particles can packed on top during the filtration

forming uniform surfaces with low surface roughness.

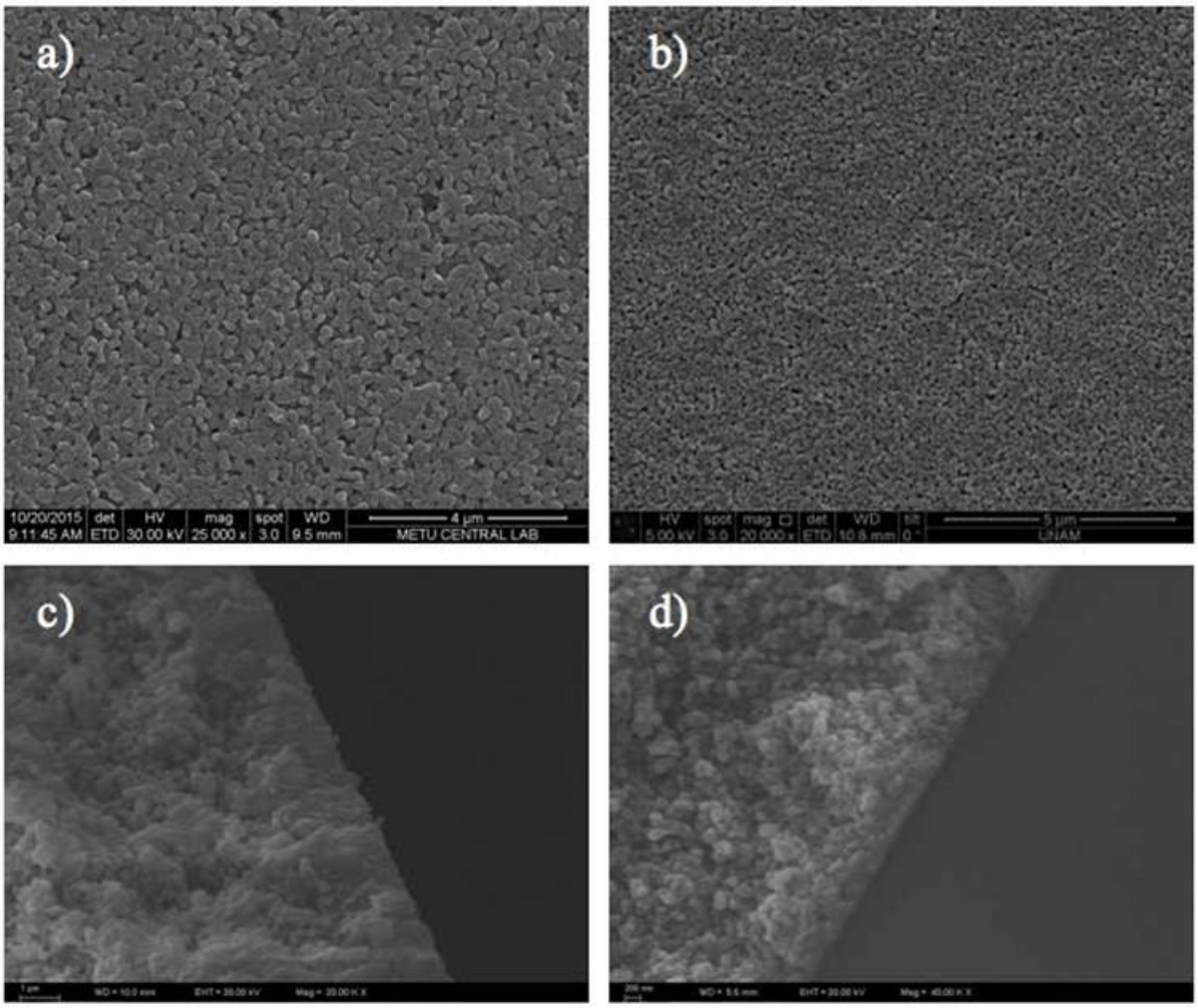

Figure 4: SEM images of the α-Al_2O_3 supports (a) top surface image of S400, (b) top surface image of S200, (c) the fracture of cross-section of S400, (d) the fracture of cross-section of S200.

Figure 5 shows SEM images of the fracture surfaces of ZnO added alumina supports with corresponding EDS spectra. ZnO added microstructure seems to have much larger surface pores. Although ZnO spheres were not observed in the structure, EDS spectra show the elemental constituents of Zn, Al, and O for both type of the supports. Addition of ZnO to the suspension results in the formation of more open structure by retaining the surface roughness sufficient for thin film coating. The presence of ZnO during the consolidation (vacuum filtration) may affect the packing behavior of alumina particles. However, additional porosity might be related to the dissolution of ZnO spheres in the alumina suspension at pH 2. Since ZnO is an amphoteric oxide, it can easily be dissolved in both acids and bases. It has been reported that ZnO particles could be dissolved completely at pH 1 was observed (18). Therefore, ZnO may behave as a pore-forming agent in the support structure by creating new pores after dissolution.

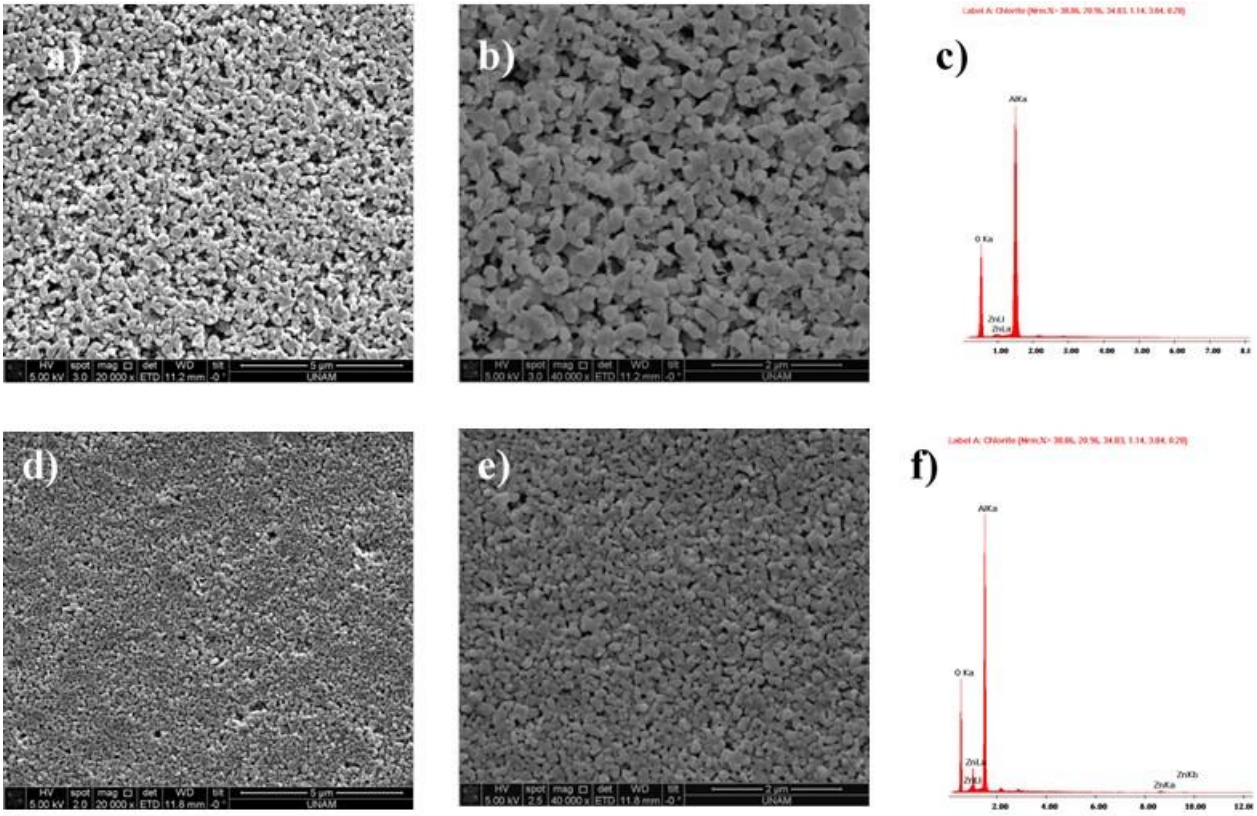

Figure 5: SEM images of ZnO added α-Al_2O_3 supports (a) top surface image of S400-Z (20kX), (b) top surface image of S400-Z (40kX), (c) corresponding EDS spectrum of S400-Z, (d) top surface image of S200-Z (20kX), (e) top surface image of S200-Z (40kX), (f) corresponding EDS spectrum of S200-Z.

The membrane supports prepared by vacuum-assisted colloidal filtration had smooth and homogeneous surface microstructure and well suited for the fabrication of the thin film. The microstructure consists of a random close packing of a smaller particle size led to slightly improved surface uniformity (Figure 4b). However, because of well packed support microstructure, these supports have relatively low permeance based on the targets for inorganic membranes (2). S400 and S200 supports at room temperature, had He permeance values of $5x10^{-6}$ mol/(m^2sPa) and $1.3x10^{-6}$ mol/(m^2sPa), respectively (Figure 6). These values are 8 and 2 times lower than the desired target value of $1x10^{-5}$ mol/(m^2sPa). In Figure 6, the He permeance of prepared supports (S400, S200, S400-Z and S200-Z) is given as a function of transmembrane pressure. From this figure, it is clear that the gas resistance of S400 support is 3 times lower compared to that for S200 support. The difference in permeance values can be explained by the difference in the pore sizes and porosity of two supports. The S400 and S200 supports had total Hg-intrusion porosities of 0.30 with 160 nm pores and 0.25 with 100 nm pores, respectively.

He permeance value has increased significantly upon addition of ZnO. S400-Z support has a He permeance in a range of $8.5\text{-}8.7x10^{-6}$ mol/(m^2sPa) which is very close to the desired

value of $1x10^{-5}$ mol/(m^2sPa). However, the permeance enhancement was not significant for S200-Z support. He permeance increased from $1.3x10^{-6}$ mol/(m^2sPa) to $1.7x10^{-6}$ mol/(m^2sPa) at 1 bar. The increase in ZnO content in S200 may lead to a stronger effect on the permeance. He permeances through the supports showed slight pressure dependence that indicated the contribution of viscous flow to the Knudsen flow.

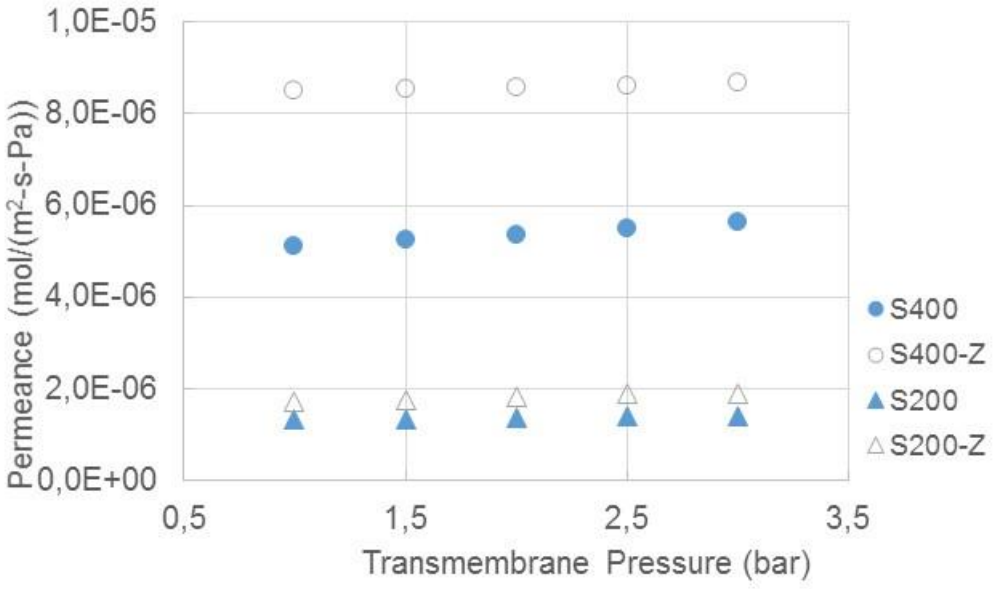

Figure 6: Effect of transmembrane pressure on He permeances at 25 °C.

The addition of ZnO improved the permeances of N_2 and CO_2 as well. Figure 7 shows the single gas permeances of He, N_2 and CO_2 for the prepared supports. The highest permeance values were obtained for S400-Z supports. Knudsen selectivities of He/CO_2 and He/N_2 are 3.3 and 2.65, respectively. All prepared supports had almost the same He/CO_2 and He/N_2 ideal selectivities with a small positive or negative deviation from Knudsen selectivities (Table 2). As a result, ZnO enabled us to increase the support flux by modifying pore structure of S400-Z but less notable influence on S200-Z support flux has been observed.

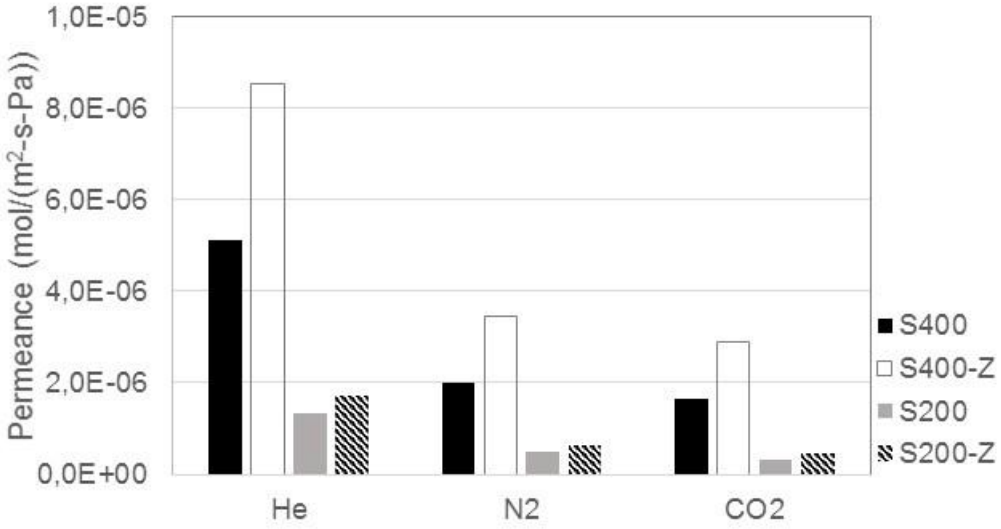

Figure 7: He, N_2 and CO_2 permeances of supports at 25 °C and 1 bar.

Table 2: He/N_2 and He/CO_2 ideal and Knudsen selectivities

Support Code	He/N_2	He/CO_2	(He/N_2)$_{KD}$	(He/CO_2)$_{KD}$
S400	2.60	3.10	2.65	3.30
S400-Z	2.50	2.95		
S200	2.80	3.95		
S200-Z	2.80	3.70		

He permeances through the supports as a function of temperature are given in Figure 8. He permeance decreased with decreasing temperature. Knudsen flow effect can be observed in these figures since He permeance for all prepared supports had inverse temperature dependence.

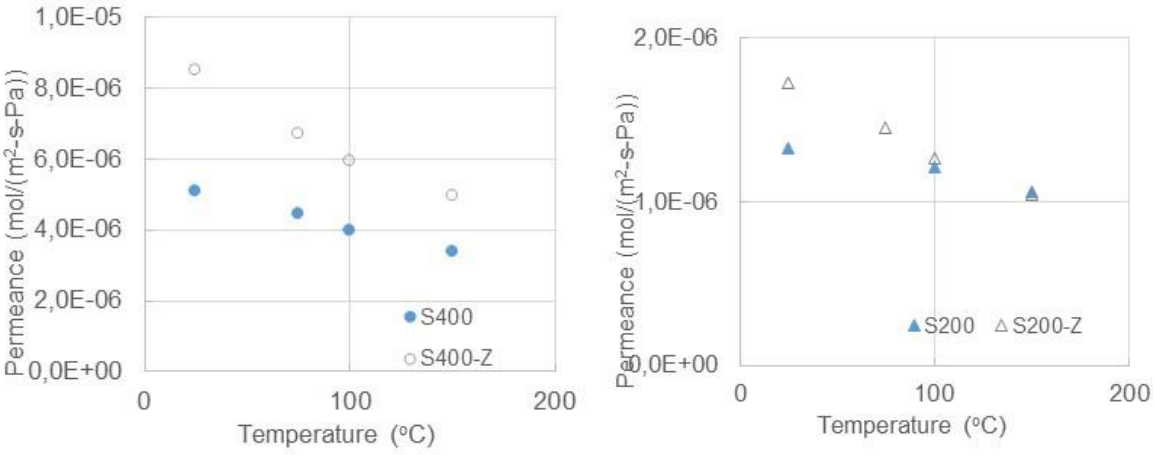

Figure 8: (a) He permeances through S400 and S400-Z (left) and S200 and S200-Z supports (right) as a function of temperature.

The Knudsen transport is valid for the pores mostly in mesoporous range between 10 nm and 100 nm, while the viscous flow is dominant in large pores. When the mean free path is comparable to pore size (at intermediate pore size) both viscous and Knudsen flow are significant (19). Since the pore size of the supports exceed 100 nm and observed slight pressure dependency in He permeance He (Figure 6), both Knudsen and viscous flow can be considered to describe the transport mechanism in the supports;

$$F = -\frac{1}{RTl}\left(D_{Kn} + \frac{B_0}{\eta}P_m\right) \quad \text{(Eq. 1)}$$

where, F is the permeance, R is the gas constant, T is the absolute temperature, *l* is the support thickness, P_m is the average pressure across the support, η is the viscosity. D_{Kn}[1] (Knudsen diffusivity) and B_o[2] include structural parameters like ε (porosity), d_p (pore diameter) and τ (tortuosity). From Eqn. 1, plotting *F* versus P_m should result in a straight line where intercept and the slope is represented by the contribution of Knudsen flow and viscous flow, respectively. If the Eqn. 1 is rearranged and plotting $Rl(MT)^{0.5}F$ versus $(M/T)^{0.5}$ P_m/η gives a straight line in which the structural factors of K_o and B_o can be obtained from intercept and slope, respectively (*M* is the molecular weight of the gas molecule). Figure 9 shows the change in $RL(MT)^{0.5}F$ with $(M/T)^{0.5}$ P_m/η obtained from N_2 permeance at temperature of 25°C through the supports and the corresponding linear fitting (R^2>0.98). The linear increase in the N_2 permeances with mean pressure was observed. In Table 3, calculated structural parameters (K_o and B_o) are given for the prepared supports. Differences in the structural parameters indicated that different pore structure formed for all prepared support. The flow induced pore diameter of S200 support was calculated as 115 nm by assuming cylindrical pores which is in agreement with the value of the pore size determined by Hg intrusion measurement (110 nm). Calculated tortuosity (2.3) is also reasonable by using the porosity of 0.25 obtained from Hg-intrusion. Although 2 times higher pore diameter was calculated for S400 support, almost the same tortuosity (2.5) value was calculated by using the Hg-intrusion porosity of 0.3. A higher flow induced pore diameter might be the result of broad pore size distribution o S400 support. Almost same structural parameters obtained for S200 and S200-Z may indicate the small change in porous network upon adding ZnO as confirmed also by small change in gas permeances for both support. The increase in permeance values for S400-Z may be the result of the

1 $D_{Kn} = \frac{4}{3}K_0 u$ where K_o $(\frac{1}{4}\frac{\varepsilon}{\tau}d_p)$ is the structural factor and *u* is the mean molecular velocity.

2 $B_0 = \frac{\varepsilon}{\tau}\frac{{d_p}^2}{32}$

increase in viscous flow contribution to the gas transport resulting low flow induced pore diameter.

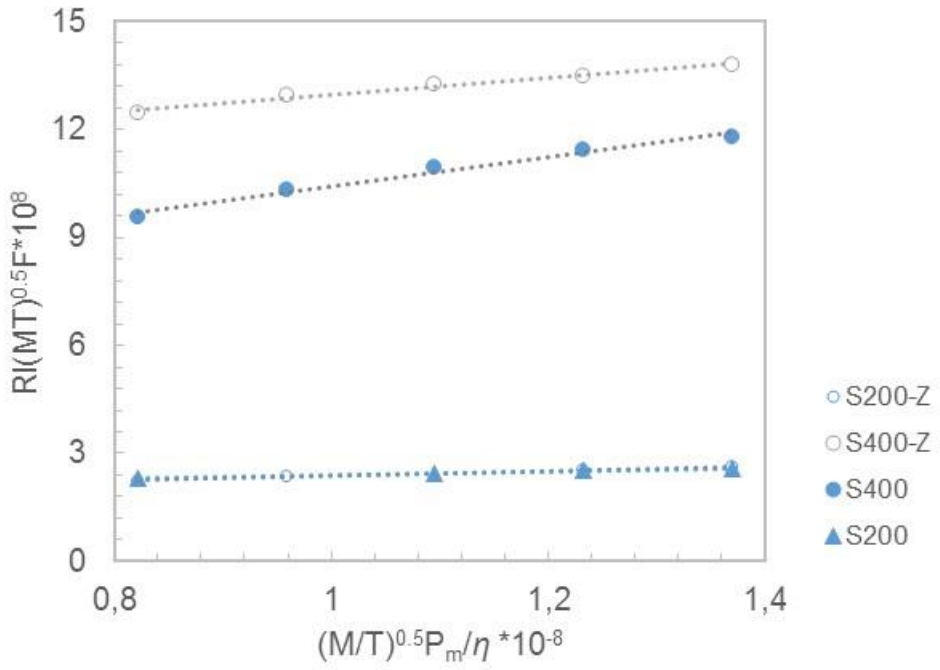

Figure 9: The change in $RL(MT)^{0.5}F$ with $(M/T)^{0.5}\,P_m/\eta$ obtained from N_2 permeance at 25 °C.

Table 3: Structural parameters obtained from permeance measurements.

Support Codes	B_o [10^{17}] m^2	K_o [10^9] m	D_p (nm)	$\frac{\varepsilon}{\tau}$ [-]
S400	40	10.3	315	0.13
S200	4.5	3.2	115	0.11
S400-Z	33	22.6	130	0.42
S200-Z	6.7	2.8	195	0.06

CONCLUSIONS

High-flux macroporous supports with macro-defect free surfaces were successfully prepared by using vacuum-assisted colloidal filtration of alumina suspensions with different particle sizes. The microstructure consists of a random close packing of 200 nm particles led to improved surface uniformity and roughness. However, these supports (S200 and S200Z) exhibited higher gas resistant compared to those prepared with larger particle size. ZnO addition enhanced the He permeance significantly for S400-Z support, but did not affect considerably for S200-Z support. Further research on the influence of added ZnO amount on gas permeances may be clarified the understanding of gas permeation behavior and microstructural changes upon ZnO addition.

ACKNOWLEDGMENTS

This study was supported by The Scientific and Technological Research Council of Turkey (TUBITAK) with project number 214M165.

REFERENCES

1. Sholl DS, Lively RP. Seven chemical separations to change the world. Nature. 2016; 532:435-7.

2. Mottern ML, Shqau K, Shi JY, Yu D, Verweij H. Thin supported inorganic membranes for energy-related gas and water purification. International Journal of Hydrogen Energy. 2007; 32(16):3713-23.

3. Agrawal KV, Topuz B, Pham TCT, Nguyen TH, Sauer N, Rangnekar N, et al. Oriented MFI Membranes by Gel-Less Secondary Growth of Sub-100 nm MFI-Nanosheet Seed Layers. Advanced Materials. 2015;27(21):3243-9.

4. Zhou H, Korelskiy D, Sjöberg E, Hedlund J. Ultrathin hydrophobic MFI membranes. Microporous and Mesoporous Materials. 2014;192:76-81.

5. de Vos RM, Verweij H. High-Selectivity, High-Flux Silica Membranes for Gas Separation. Science. 1998;279(5357):1710-1.

6. van Veen HM, Rietkerk MDA, Shanahan DP, van Tuel MMA, Kreiter R, Castricum HL, et al. Pushing membrane stability boundaries with HybSi® pervaporation membranes. Journal of Membrane Science. 2011;380(1):124-31.

7. Bissett H, Zah J, Krieg HM. Manufacture and optimization of tubular ceramic membrane supports. Powder Technology. 2008;181(1):57-66.

8. Mottern M, Chiu W, Warchol Z, Shqau K, Verweij H. High-performance membrane supports: A colloidal approach to the consolidation of coarse particles. International Journal of Hydrogen Energy. 2008;33(14):3903-14.

9. Chang CH, Gopalan R, Lin YS. A comparative study on thermal and hydrothermal stability of alumina, titania and zirconia membranes. Journal of Membrane Science. 1994;91(1–2):27-45.

10. Larbot A, Alami-Younssi S, Persin M, Sarrazin J, Cot L. Preparation of a γ-alumina nanofiltration membrane. Journal of Membrane Science. 1994;97:167-73.

11. Bruni YL, Garrido LB, Aglietti EF. Effect of high alumina cement on permeability and structure properties of ZrO2 composites. Ceramics International. 2012; 38(3):1755-63.

12. Shojai F, Mäntylä T. Monoclinic Zirconia Microfiltration Membranes: Preparation and Characterization. Journal of Porous Materials. 8(2):129-42.

13. Van Gestel T, Vandecasteele C, Buekenhoudt A, Dotremont C, Luyten J, Leysen R, et al. Alumina and titania multilayer membranes for nanofiltration: preparation, characterization and chemical stability. Journal of Membrane Science. 2002; 207(1):73-89.

14. Cesarano J, Aksay IA. Processing of Highly Concentrated Aqueous α-Alumina Suspensions Stabilized with Polyelectrolytes. Journal of the American Ceramic Society. 1988;71(12):1062-7.

15. Agrawal KV, Topuz B, Jiang Z, Nguenkam K, Elyassi B, Francis LF, et al. Solution-processable exfoliated zeolite nanosheets purified by density gradient centrifugation. AIChE Journal. 2013; 59(9):3458-67.

16. Lin L, Zhang T, Liu H, Qiu J, Zhang X. In situ fabrication of a perfect Pd/ZnO@ZIF-8 core-shell microsphere as an efficient catalyst by a ZnO support-induced ZIF-8 growth strategy. Nanoscale. 2015;7(17):7615-23.

17. Lewis JA. Colloidal processing of ceramics. Journal of the American Ceramic Society. 2000;83(10):2341-59.

18. Mudunkotuwa IA, Rupasinghe T, Wu C-M, Grassian VH. Dissolution of ZnO Nanoparticles at Circumneutral pH: A Study of Size Effects in the Presence and Absence of Citric Acid. Langmuir. 2012;28(1):396-403.

19. Gao X, Bonilla MR, Costa JCDd, Bhatia SK. The transport of gases in macroporous α-alumina supports. Journal of Membrane Science. 2012; 409-410:24-33.